Available online at www.sciencedirect.com
SCIENCE DIRECT®
Journal of Solid State Chemistry 178 (2005) 1445–1451
JOURNAL OF SOLID STATE CHEMISTRY
www.elsevier.com/locate/jssc

Syntheses of fluorescent thiocyanate supramolecular compounds with unusual two-dimensional structures

Hai-Ying Bie, Jing Lu, Jie-Hui Yu, Ji-Qing Xu*, Kui Zhao, Xiao Zhang

College of Chemistry and State Key Laboratory of Inorganic Synthesis and Preparative Chemistry, Jilin University, Changchun 130023, Jilin Province, P.R. China

Received 28 December 2004; received in revised form 28 January 2005; accepted 28 January 2005
Available online 17 March 2005

Abstract

Three novel thiocyanate supramolecular compounds have been synthesized and characterized by X-ray diffraction and fluorescent spectra. Compound $[pipH]_2[Co(NCS)_4]$ (pip = piperazine) **1** possesses a two-dimensional layer connected by the combination of N–H···N hydrogen bonds and weak S···S contacts. Under the same conditions, using nickel salt instead of cobalt salt as a starting material, we obtained a different two-dimensional supramolecular layer $[pipH]_2[Ni(NCS)_4]$ **2** connected by unusual N–H···S hydrogen bonds and weak S···S contacts. In order to observe the influence of the dimension of ligand on the self-assembly structure, dabco was used for substituting pip, and compound $[dabcoH]_2[Ni(NCS)_4]$ (dabco = 1,4-Diazabicyclo[2.2.2] octane) **3** was gained, which constructed two-dimensional, highly wavy network with hourglass-shaped cavities only through N–H···S hydrogen bonds.

Keywords: Supramolecular compounds; Hydrogen bonds; S···S contacts; Crystal engineering; Thiocyanate; Fluorescence

1. Introduction

Great interest has recently been focused on the crystal engineering of coordination frameworks due to their fascinating architectures and potential applications as functional materials in catalysis, magnetism, superconductor and non-linear optical materials [1]. In the construction of such supramolecular materials, one important strategy is those of low-dimensional metal-containing building blocks extended to high-dimensional networks through weak intermolecular interactions, including hydrogen-bonding, $\pi\cdots\pi$ stacking and weak van der Waals interactions, etc. Doubtless, the hydrogen bond is the most familiar organizing force in supramolecular assemblies by virtue of its unique strength and directionality that may control short-range packing [2]. Many research groups have paid attention to the studies of the hydrogen bonds [3]. For example, Munakata has reported controlling the three-dimensional supramolecular channel-like copper compounds hosting a variety of anions by changing the hydrogen-bonding modes and distances [4]. However, other supramolecular interactions, such as weak van der Waals interaction, have been less documented and only few examples generated by the combination of multi-supramolecular interactions have been reported [5]. Our three-fold strategy was to select thiocyanate group: (a) Considering the varieties of coordination modes, SCN^- is a highly versatile ligand with two donor atoms. It can coordinate through either nitrogen or sulfur atom, or both, giving rise to linkage isomers or polymers [6]. (b) It can provide hydrogen bond acceptors with nitrogen or sulfur atom. (c) Sulfur atoms can form weak van der Waals S···S interaction. In this paper, we reported three new thiocyanate supramoelcular architectures, namely $[pipH]_2[Co(NCS)_4]$ (pip = piperazine) **1**, $[pipH]_2[Ni(NCS)_4]$ **2** and $[dabcoH]_2[Ni(NCS)_4]$ (dabco = 1,4-

*Corresponding author. Fax: +86 431 8499158.
E-mail address: xjq@mail.jlu.edu.cn (J.-Q Xu).

0022-4596/$ - see front matter © 2005 Elsevier Inc. All rights reserved.
doi:10.1016/j.jssc.2005.01.027

Diazabicyclo[2.2.2] octane) **3**, constructed by the combination of coordination bonds, hydrogen bonds and weak van der Waals interactions.

2. Experimental section

2.1. Materials and physical measurements

All reagents were commercially available and used as received. Infrared spectra were recorded as a KBr pellet with Perkin-Elmer spectrophotometer in the 200–4000 cm^{-1} region. The elemental analyses for C, H and N were determined using a Perkin-Elmer 2400 LS II elemental analyzer. Fluorescent properties were measured using FS900 Eding Burgh instrument.

2.2. Syntheses

2.2.1. Synthesis of *[pipH]$_2$[Co(NCS)$_4$]* **1**

Single crystals were grown in a solution at room temperature. A methanol solution (5 mL) of pip (0.19 g, 1.0 mmol) was added dropwise into an aqueous solution (10 mL) of $Co(NO_3)_2 \cdot 6H_2O$ (0.29 g, 1.0 mmol) and NH_4NCS (0.30 g, 4.0 mmol), and then pH = 5 was adjusted with concentrated HCl solution. Red crystals were obtained in yield ≈20% after the filtrate was allowed to stand for 1 week. IR (cm^{-1}): 3233(m), 3119(m), 2089(vs), 2045(vs), 2023(vs), 1559(s), 1468(m), 1448(m), 1416(s), 1327(w), 1300(w), 1214(m), 1202(m), 1099(vs), 1067(vs), 991(vs), 875(vs), 812(w), 791(m), 613(s), 478(s), 469(s), 427(m), 316(m). Anal. Calcd. for $C_{12}H_{22}CoN_8S_4$ (%): C, 30.96; H, 4.76; N, 24.08. Found: C, 30.75; H, 4.73; N, 24.21.

2.2.2. Synthesis of *[pipH]2[Ni(NCS)$_4$]* **2**

Single crystals were prepared using the same treatment as **1** with $NiCl_2 \cdot 6H_2O$ (0.24 g, 1.0 mmol) instead of $Co(NO_3)_2 \cdot 6H_2O$. Green crystals were obtained in yield ≈60% after the filtrate was allowed to stand for several days. IR (cm^{-1}): 3216(m), 2948(m), 2752(w), 2455(w), 2110(vs), 1649(w), 1586(s), 1459(m), 1446(m), 1403(s), 1371(w), 1294(m), 1213(m), 1198(m), 1142 (m), 1096(vs), 1062(m), 1025(m), 999(s), 870(s), 813(w), 783(w), 773(w), 469(s), 460(s), 430(m), 326(m). Anal. Calcd. for $C_{12}H_{22}NiN_8S_4$ (%): C, 30.97; H, 4.76; N, 24.09. Found: C, 30.66; H, 4.73; N, 24.24.

2.2.3. Synthesis of *[dabcoH]$_2$[Ni(NCS)$_4$]* **3**

Compound **3** was prepared similar to **2**, using dabco (0.11 g, 1.0 mmol) instead of pip. Green crystals were obtained in yield ≈40% after the filtrate was allowed to stand for several days. IR (cm^{-1}): 2974(m), 2829(w), 2783(w), 2625(w), 2111(vs), 2082(vs), 1461(s), 1402(m), 1314(m), 1240(m), 1173(w), 1048(s), 997(m), 956(w), 1099(vs), 902(m), 843(s), 805(w), 794(m), 780(s), 604(s), 475(s), 414(m), 329(m). Anal. Calcd. for $C_{16}H_{26}N_8NiS_4$ (%): C, 37.14; H, 5.07; N, 21.66. Found: C, 37.04; H, 4.98; N, 21.56.

2.3. X-ray crystal structure determination

Crystallographic data for these three compounds are summarized in Table 1. The data were collected with

Table 1
Crystallographic data and structure refinement for compounds **1**, **2** and **3**

	1	**2**	**3**
Empirical formula	$C_{12}H_{22}CoN_8S_4$	$C_{12}H_{22}NiN_8S_4$	$C_{16}H_{26}N_8NiS_4$
Formula weight	465.54	465.32	517.40
Crystal system	Monoclinic	Monoclinic	Monoclinic
Space group	$P2_1/n$	$P2_1/n$	$P2_1/n$
Unit cell dimension	$a = 6.7778(14)$ Å	$a = 7.4098(11)$ Å	$a = 7.180(2)$ Å
	$b = 11.876(2)$ Å	$b = 11.0184(17)$ Å	$b = 11.198(3)$ Å
	$\beta = 101.57(3)^\circ$	$\beta = 96.738(3)^\circ$	$\beta = 96.89(3)^\circ$
	$c = 12.110(2)$ Å	$c = 12.3042(19)$ Å	$c = 14.348(6)$ Å
Volume, Z	954.9(3) $Å^3$, 4	997.6(3) $Å^3$, 4	1145.3(7) $Å^3$, 4
Density	1.619 g/cm^3	1.549 g/cm^3	1.500 g/cm^3
$F_{(000)}$	482	484	540
Absorption coefficient	1.350 mm^{-1}	1.405 mm^{-1}	1.232 mm^{-1}
Crystal size	0.23 × 0.20 × 0.05 mm^3	0.20 × 0.15 × 0.10 mm^3	0.45 × 0.20 × 0.20 mm^3
θ range	2.43–25.05°	2.49–28.09 °	2.31–25.09°
Limiting indices	$-5 \leqslant h \leqslant 8$, $-8 \leqslant k \leqslant 12$, $-14 \leqslant l \leqslant 3$	$-9 \leqslant h \leqslant 9$, $-14 \leqslant k \leqslant 13$, $-9 \leqslant l \leqslant 15$	$-8 \leqslant h \leqslant 8$, $-13 \leqslant k \leqslant 10$, $-7 \leqslant l \leqslant 17$
T (K)	293 (2)	293 (2)	293 (2)
Data/restraints/parameters	1329/0/123	2238/0/115	1971/0/134
Goodness of fit indicator	0.941	1.019	1.047
Final R indicates [$I > 2\sigma(I)$]	$R_1 = 0.0360$, w$R_2 = 0.0722$	$R_1 = 0.0317$, w$R_2 = 0.0773$	$R_1 = 0.0506$, w$R_2 = 0.1315$
Largest diff. peak and hole	0.257 and −0.276 e/$Å^3$	0.294 and −0.407 e/$Å^3$	0.841 and −0.809 e/$Å^3$

Table 2
Selected bonds length (Å) and angles (deg) for compounds **1**, **2** and **3**

1		**2**		**3**	
Co(1)–N(2)	2.221(3)	Ni(1)–N(3)	2.0690(19)	Ni(1)–N(1)	2.300(4)
Co(1)–N(3)	2.087(4)	Ni(1)–N(4)	2.0765(16)	Ni(1)–N(3)	2.044(4)
Co(1)–N(4)	2.194(4)	Ni(1)–N(2)	2.1941(14)	Ni(1)–N(4)	2.054(4)
N(3)–Co(1)–N(3)#1	180.000(1)	N(3)#1–Ni(1)–N(3)	180.00(12)	N(3)–Ni(1)–N(3)#1	180.000(1)
N(3)–Co(1)–N(4)#1	87.81(14)	N(3)#1–Ni(1)–N(4)	89.48(7)	N(3)–Ni(1)–N(4)#1	89.34(16)
N(3)–Co(1)–N(4)	92.19(14)	N(3)–Ni(1)–N(4)	90.52(7)	N(3)–Ni(1)–N(4)	90.66(16)
N(4)#1–Co(1)–N(4)	180.0	N(4)–Ni(1)–N(4)#1	180.00(13)	N(4)#1–Ni(1)–N(4)	180.0
N(3)–Co(1)–N(2)	93.13(12)	N(3)#1–Ni(1)–N(2)	89.12(6)	N(3)–Ni(1)–N(1)#1	90.23(14)
N(3)#1–Co(1)–N(2)	86.87(12)	N(3)–Ni(1)–N(2)	90.88(6)	N(3)#1–Ni(1)–N(1)#1	89.77(14)
N(4)#1–Co(1)–N(2)	86.45(12)	N(4)–Ni(1)–N(2)	88.33(6)	N(4)#1–Ni(1)–N(1)#1	93.48(15)
N(4)–Co(1)–N(2)	93.55(12)	N(4)#1–Ni(1)—N(2)	91.67(6)	N(4)–Ni(1)–N(1)#1	86.52(15)
N(2)–Co(1)–N(2)#1	180.000(1)	N(2)–Ni(1)–N(2)#1	180.00(9)	N(1)#1–Ni(1)–N(1)	180.000(1)
C(3)–N(2)–Co(1)	117.8(2)	C(3)–N(2)–Ni(1)	109.93(14)	C(3)–N(1)–Ni(1)	112.3(3)
C(2)–N(2)–Co(1)	114.9(2)	C(2)–N(2)–Ni(1)	114.03(11)	C(1)–N(1)–Ni(1)	110.9(3)
C(6)–N(4)–Co(1)	130.0(3)	C(6)–N(4)–Ni(1)	170.97(16)	C(7)–N(3)–Ni(1)	176.8(4)
C(5)–N(3)–Co(1)	164.5(4)	C(5)–N(3)–Ni(1)	176.96(18)	C(8)–N(4)–Ni(1)	150.6(4)
N(4)–C(6)–S(2)	177.7(3)	N(3)–C(5)–S(1)	178.75(19)	N(3)–C(7)–S(1)	178.7(5)
N(3)–C(5)–S(1)	178.4(4)	N(4)–C(6)–S(2)	179.15(18)	N(4)–C(8)–S(2)	178.1(5)

Symmetry transformations used to generate equivalent atoms: #1, $-x$, $-y$, $-z+1$ (for compound **1**); #1, $-x$, $-y$, $-z$ (for compound **2**); #1, $-x+1$, $-y+1$, $-z+1$ (for compound **3**).

MoKα radiation ($\lambda = 0.71073$ Å) using a Siemens SMART CCD diffractometer at 293(2) K. The crystal class, orientation matrix, and cell dimensions were determined according to established procedures [7]. Absorption corrections were applied using SADABS. The structures were solved using direct methods with SHELXTL program and refined by full-matrix least-squares techniques. The non-hydrogen atoms were assigned anisotropic displacement parameters in the refinement. The hydrogen atoms were treated using a riding model (Table 2).

3. Results and discussion

3.1. Description of the crystal structures of 1–3

3.1.1. Crystal structure of complex 1

As shown in Fig. 1, the coordination polyhedron of **1** is defined by six nitrogen atoms around the cobalt atom in a slightly distorted octahedral geometry. The equatorial plane is constituted by four nitrogen atoms [N(3), N(3A), N(4), N(4A)] belonging to the four thiocyanate groups while the apical positions are occupied by two nitrogen atoms [N(2), N(2A)] from two pip ligands. The Co–N bond lengths involving the NCS^- groups [2.087(4) and 2.194(4) Å, for N(3) and N(4), respectively] are shorter than those involving the pip ligands [2.221(3) Å for N(2)] and this fact is observed in other compounds of cobalt thiocyanate and amide ligands, such as the known coordination polymer $[Co(NCS)_2(bbbt)_2]$ (bbbt = 1,1′-(1,4-butanediyl) bis-1H-benzotriazole) [8]. The thiocyanate groups are almost linear with the angles [N(4)–C(6)–S(2), 177.7(3) and N(3)–C(5)–S(1), 178.4(4)°], which conform to the typical values being in the 175–178° range [9], whereas a significant bending is displayed by Co–N–C(S) linkages, which deviate from 180° expected for the sp hybrid orbital of the N atom. Because the Co–N(4)–C(6) angle of 130.0(3)° implies less over lap between the sp hybrid orbital of the N atom and the atomic orbital of Co(II) than that of C(5)–N(3)–Co(1), 164.5(4)°, the Co–N(4) distance [2.194(4) Å] is apparently longer than the Co–N(3) distance [2.087(4) Å].

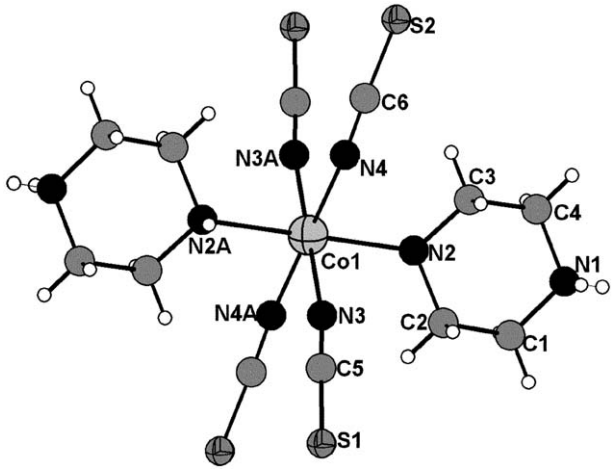

Fig. 1. The coordination environment of monomeric unit **1**.

Two of the four thiocyanate groups in each discrete structural unit participate in N–H···N hydrogen bonds with the neighboring protonated piperazine

cations. It is these strong hydrogen bonded interactions [N(1)–H(1A)···N(4) = 2.16(6) Å] that make these neighboring monomeric units assembled into a one-dimensional hydrogen-bonded chain along the *c*-axis. The most important feature in the supramolecular compound **1** is the role of the sulfur atoms. Each sulfur atom of the one-dimensional hydrogen-bonded chain has a weak S···S interaction with a sulfur atom from an adjacent chain along the *b*-axis (Fig. 2). The distances of S···S contact, being 3.664(4) Å, are slightly shorter than the sum of the van der Walls radii of two sulfur atoms, indicating the existence of weak interactions. With these S···S interactions, the self-assembled one-dimensional chain further extends to a two-dimensional supramolecular layer, that is, the monomeric units associate with each other through the combination of coordination bonds, hydrogen bond N–H···N interactions and S···S contacts.

3.1.2. Crystal structure of complex **2**

Under the same conditions, using the nickel (II) salt instead of cobalt (II) salt as a starting material, we obtained compound $[pipH]_2[Ni(NCS)_4]$ **2**, in which the monomeric structure of the nickel atom is similar to that of **1**. However, no heavy bending is displayed by Ni–N–C(S) linkages [C(6)–N(4)–Ni(1), 170.97(16)° and C(5)–N(3)–Ni(1), 176.96(18)°, respectively], which is different from **1**, so the Ni–N(3) distance [2.072(2) Å] is similar to the Ni–N(4) distance [2.0758(18) Å].

It is worth noting that different weak intermolecular interaction patterns of unusual N–H···S hydrogen bonds and S···S contacts exist. As shown in Fig. 3(a), each monomeric unit is connected by two N–H···S intermolecular hydrogen bonds N(1)–H(1A)···S(1) = 2.526 Å, forming one-dimensional chains in one direction. At the same time, in the other direction there also exist N–H···S hydrogen bonds. It is these hydrogen bonds that make the one-dimensional chains assembled into two-dimensional, highly wavy networks concentrated about the (100) planes with hourglass-shaped cavities (ca. 14.2 Å long, 8.7 Å wide at the ends, and 7.8 Å at the waist). It is interesting not only because it forms a large hourglass-shaped cavity, but also because hydrogen-bonded networks via sulfur acceptors are still less explored until now [10]. As displayed in Fig. 3(b), each sulfur atom in monomeric units is connected with the four neighboring units by weak S···S interactions to form a two-dimensional layer with 20-member rings. The distance of S···S contact is 3.64 Å.

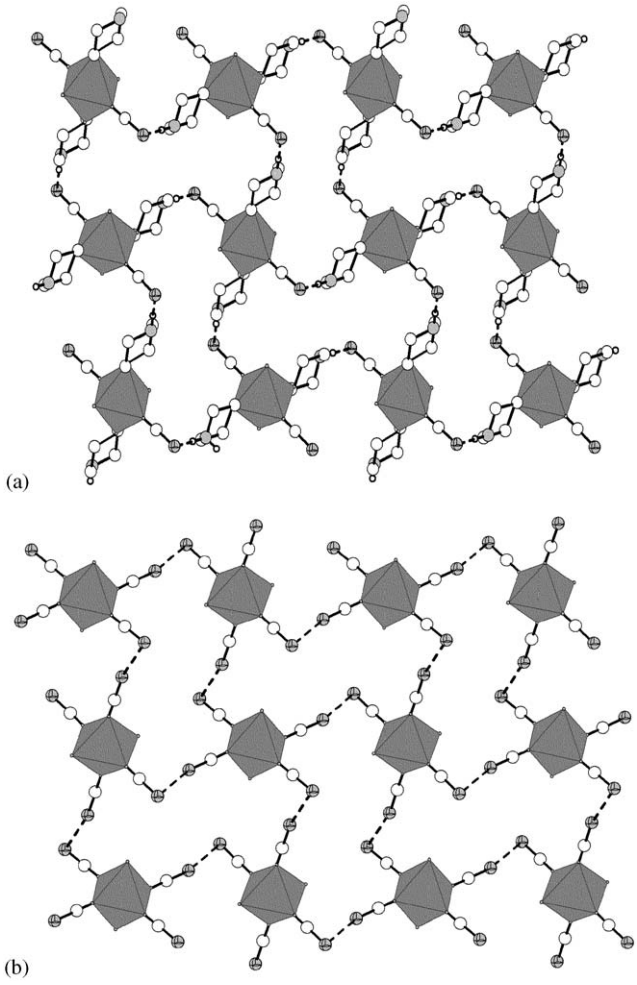

Fig. 3. (a) The two-dimensional layer with hourglass-shaped cavities constructed by unusual N–H···S hydrogen bonds (The groups which do not participate in forming hydrogen bonds were discarded for clarity), (b) the two-dimensional layer assembled only by S···S contacts (N–H···S hydrogen bonds and pip were omitted for clarity) along the a axial in **2**.

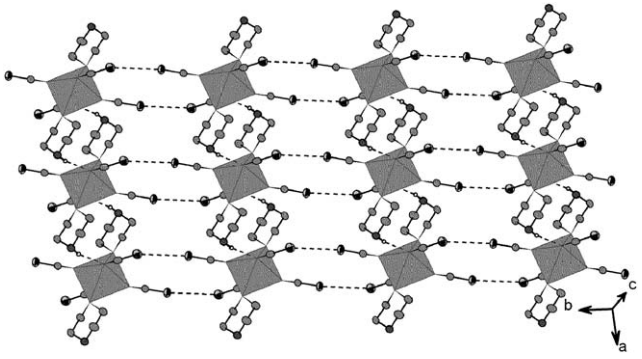

Fig. 2. The two-dimensional layer assembled through the combination of N–H···N hydrogen bonds and weak S···S interactions in **1**.

It is notable that the role of S···S contacts cannot increase the dimension of this supramolecular assembly but transform hourglass-shaped cavities into chair configuration (Fig. 4). This fact does not exist in compound **1**, in which the role of S···S contacts make one-dimensional hydrogen-bonded chain connected to form the two-dimensional layer.

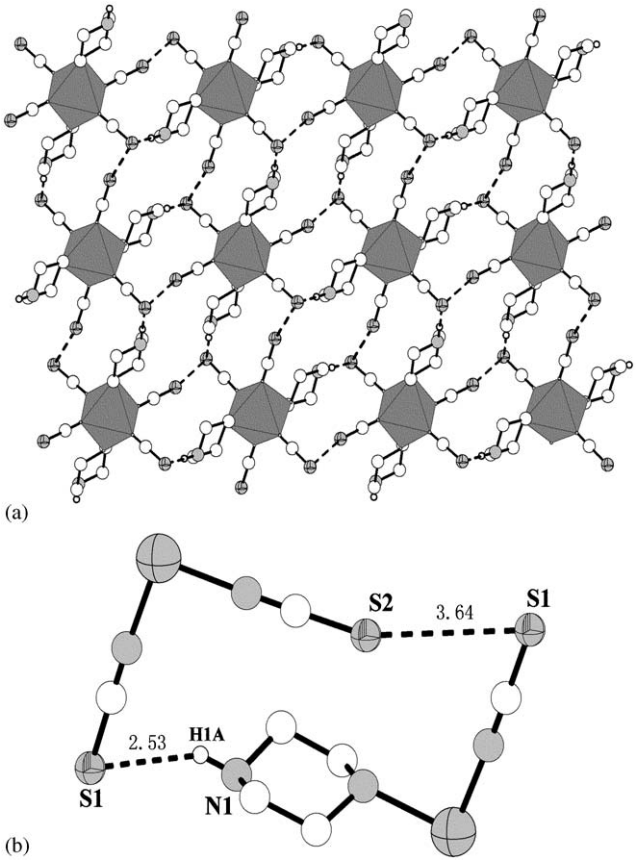

Fig. 4. The two-dimensional layer assembled through the combination of hydrogen bonds N–H···S and weak S···S interactions in **2**.

3.1.3. *Crystal structure of complex* **3**

In order to observe the influence of the dimension of ligand on the self-assembly structure, we gained $[dabcoH]_2[Ni(NCS)_4]$ **3** using dabco instead of pip. The coordination environment of the nickel atom in monomeric unit is similar to that of **1** and **2**. It is worth noting that there exists only one kind of weak interaction N–H···S hydrogen bonds. Each monomeric unit is connected by four N–H···S intermolecular hydrogen bonds (N(2)–H(2)···S(1) = 2.388(26) Å), slightly shorter than those in **2**, forming two-dimensional and highly wavy networks concentrated about the (100) planes with hourglass-shaped cavities (ca. 14.4 Å long, 9.4 Å wide at the ends, and 7.9 Å at the waist), which is slightly larger than that shown in **2**, probably because of the larger size of the ligand. It is the steric encumbrance of dabco ligand that makes the distance of S···S linkage larger than the sum of van der Walls radii and caused the rupture of S···S contacts in comparison with **2**. In addition, the effect of the larger size of the sulfur acceptors compared with the nitrogen atoms on the crystal structures is observed because for the intermolecular hydrogen bonds, the N–H···S distance in **2** and **3** is much longer than the distance N–H···N in **1**. These results indicate that NCS^- groups are of great benefit to the construction of new assembly structures not only by N–H···S(CN^-) or N–H···N(CS^-) intermolecular hydrogen bonds between metal complex units, but also by weak S···S interactions (Fig. 5).

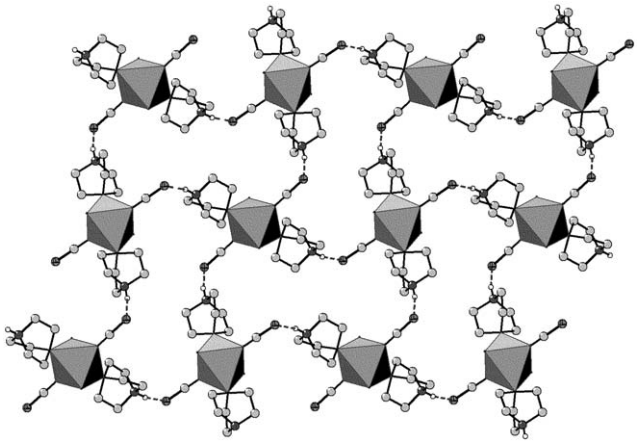

Fig. 5. The two-dimensional layer with hourglass-shaped cavities constructed by unusual N–H···S hydrogen bonds in **3** (The groups which do not participate in forming hydrogen bonds were discarded for clarity).

4. Discussion

From the comparison of packing structures between **1** and **2**, we found that under the same conditions, the difference in metal centers caused the formation of the distinct hydrogen bonds modes, N–H···N in **1**, N–H···S in **2**. Therefore, their supramolecular frameworks have great discrimination. The supramolecular structures of **2** and **3** are also different using the same metal center and different size of ligands, probably because the steric encumbrance role of the larger ligand makes the S···S linkage disappear. We have tried to obtain the adduct of $Co(NCS)_2$ and the amine dabco, but failed, perhaps this reaction condition did not suit the growth of its single-crystals. Although these monomeric units are simple, their self-assembly supramolecular structures are colorful and interesting due to the influence of the central metal ions and ligand size.

The asymmetric stretching vibrations of NCS^- in complexes **1**–**3** were observed in the range of 2023–2111 cm^{-1} as a strong band and sometimes expressively split or with a shoulder. Considering the position of the band υ_{as}(NCS), it may be assumed that the thiocyanate group is coordinated to metal atoms by its nitrogen atom, not by sulfur atom with non-bridging modes (*M*–NCS) [11]. The absorption peaks in the 400–200 cm^{-1} region were assigned to the *M*–NCS and *M*–N (L) vibrations.

4.1. Fluorescent properties

The emission spectra of **1**–**3** at room temperature are shown in Fig. 6. It can be observed that one strong emission approximately occurring at 411 nm, which was excited by the light of 350 nm for **1**, should be assigned neither to LMCT (ligand-to-metal charge transfer) nor MLCT (metal-to-ligand charge transfer) in nature and can probably be assigned to intraligand fluorescent emission, since free piperazine exhibits a similar fluorescent emission at 418 nm ($\lambda_{ex} = 312$ nm). The diagram of energy levels for **1** can be drawn according to the fluorescent property (shown in Scheme 1(1)). When it is excitated at 350 nm, the electron transfers from ground state E0 to excited state E2, then it decays to E1 energy levels in the form of non-radiative transfer, from which it comes back to the ground state E0 with light energy emission (411 nm). When it is excited at 282 nm, the electron transfers from the ground state E0 to excited state E3. Then the excitation energy completely decayed in the form of non-radiative transfer. Therefore, the excitation energy around 282 nm does not show any emission band in the metal complex.

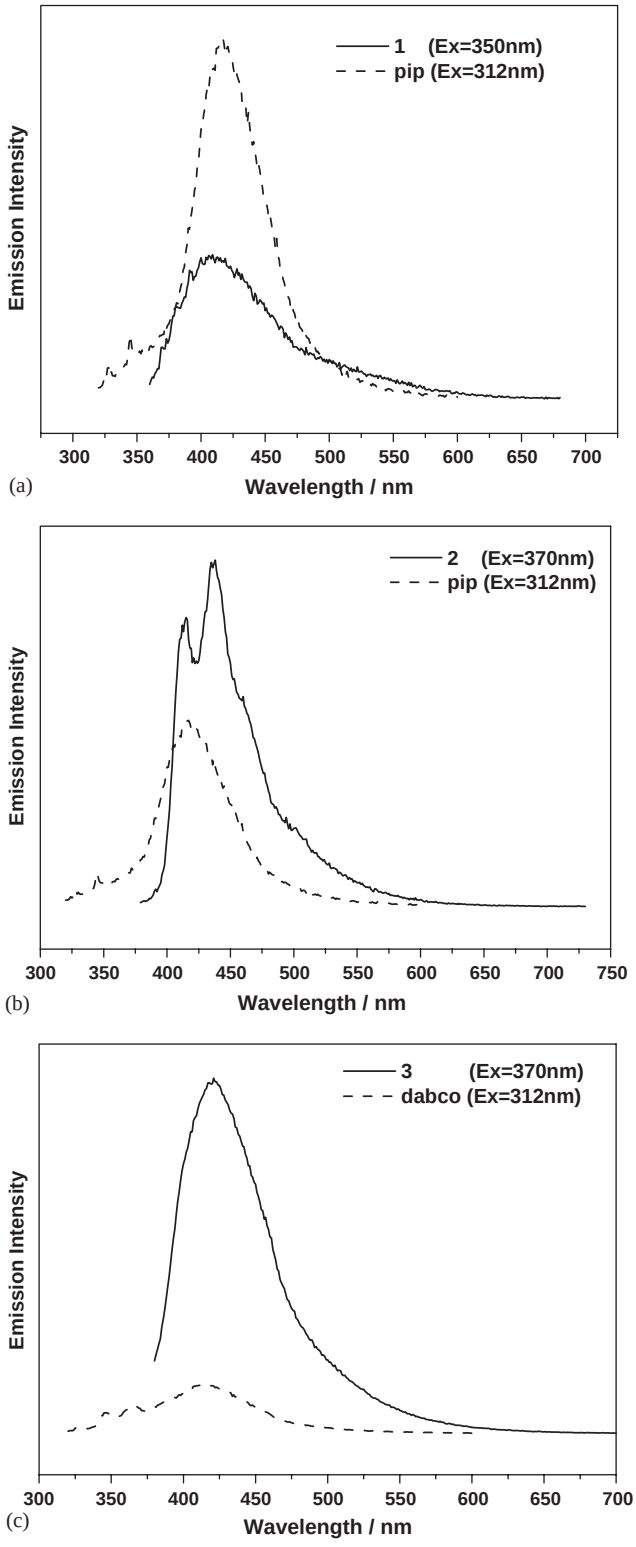

Fig. 6. The emission spectra at room temperature of compounds **1**–**3**, free pip and dabco ligands.

As shown in Fig. 6(b), the fluorescent emission band of free pip ligand is mainly located at 418 nm ($\lambda_{ex} = 312$ nm). Because the emission band of **2** is similar to that of the free pip ligand with a slight red shift, it should be assigned to the intraligand electronic transfer of pip ligand. The emission wavelength of **2** undergoes a red shift probably because the pip ligand is protonated and the energy gap between the intraligand molecular orbitals decreases. Due to the increase of the rigidity of ligand in forming the coordination bonds and reduction, the non-radiative decay of the intraligand at the excited state and the emission intensity of **2** increases, approximately two times that of free pip. The diagram of energy levels for **2** is displayed in Scheme 1(2). When it is excited at 370 nm, the electron transfers from ground state E0 to excited state E3. Then it non-radiatively decays to E2 and E1 energy levels, from which it comes back to ground state E0 with light energy emission (415 and 437 nm). It is verified by the fluorescent spectra that the chances of non-radiative decay from E3 to E1 is larger than that of non-radiative decay from E3 to E2, because the main emission peak is 437 nm.

For **3**, there is a strong emission peak at 420 nm ($\lambda_{ex} = 370$ nm), which can correspond to the intraligand fluorescent emission, since free dabco ligand displayed a similar emission at 415 nm ($\lambda_{ex} = 312$ nm). In comparison with the free dabco molecule, the energy shift in **3** was observed, undoubtedly, owing to the protonation of the ligands during the formation of supramolecular structures. It should be pointed that the emission intensity of **3** increases approximately seven times that of free dabco because of the increase in the rigidity of ligand in forming the coordination polymers and reducing the non-radiative decay of the intraligand at excited state. When it is excited at 370 nm, compound **3**

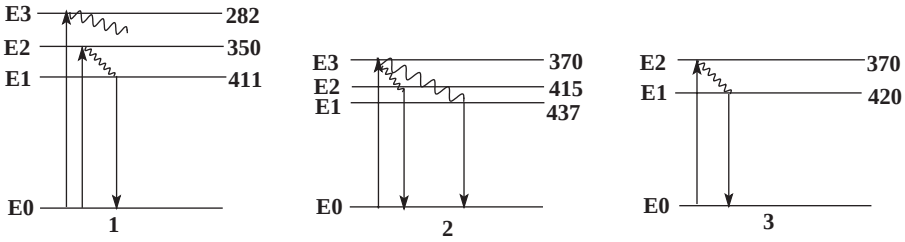

Scheme 1. View of the energy level of **1**–**3**.

exhibits a strong emission band at 420 nm. So the diagram of energy levels for **3** can be drawn in Scheme 1(3). The electron is excited from ground state to excited state E2, then it non-radiatively decays to E1, from which it comes back to ground state with the emission of 420 nm.

In conclusion, all of the compounds display fluorescent properties in the blue region at room temperature. All of the emission bands can be assigned to the intraligand electronic transfer. In comparison with the free ligands, the energy shift can originate by the protonation of the ligands during the formation of supramolecular structures.

5. Supplementary data

Supplementary data have been deposited with the Cambridge Crystallographic Centre, CCDC Nos. 232368, 249577 and 232369. Copy of this information may be obtained free of charge from The Director, CCDC, 12 Union Road, Cambridge, CB2 1EZ, UK (fax: +44-1223-336033; e-mail: deposit@ccdc.cam.ac.uk or www: http://www.ccdc.cam.ac.uk).

Acknowledgment

This research was supported by grants from the National Natural Science Foundation of China (Nos. 20271021 and 20333070).

References

[1] (a) O.R. Evans, W.B. Lin, Chem. Mater. 13 (2001) 2705;
(b) O. Astillo, A. Luque, S. Sertucha, P. Román, F. Loret, Inorg. Chem. 39 (2000) 6142;
(c) S.R. Batten, R.J. Robson, Angew. Chem. Int. Ed. 38 (1999) 2639.
[2] S.V. Kolotuchin, E.E. Fenlon, S.R. Wilson, C.J. Loweth, S.C. Zimmerman, Angew. Chem. Int. Ed 34 (1995) 2654.
[3] (a) H.J. Choi, M.P. Suh, Inorg. Chem. 38 (1999) 6309;
(b) D.P. Cheng, M.A. Khan, R.P. Houser, Inorg. Chem. 40 (2001) 6858;
(c) D.F. Sun, R. Cao, Y.Q. Sun, W.H. Bi, X.J. Li, Y.Q. Wang, Q. Shi, X. Li, Inorg. Chem. 42 (2003) 7512.
[4] M. Munakata, L.P. Wu, M. Yamamoto, T. Kuroda-Sowa, M. Maekawa, J. Am. Chem. Soc. 118 (1996) 3117.
[5] H.J. Chen, L.Z. Zhang, Z.G. Cai, G. Yang, X.M. Chen, J. Chem. Soc. Dalton Trans. 45 (2000) 2463.
[6] (a) L. Shen, Y.Z. Xu, J. Chem. Soc. Dalton Trans. (2001) 3413;
(b) H. Krautscheid, N. Emig, N. Klaassen, P. Seringer, J. Chem. Soc. Dalton Trans. (1998) 3071;
(c) E.Q. Gao, Z.M. Wang, C.H. Yan, Chem. Commun. 45 (2003) 1748.
[7] Software package SMART and SAINT, Siemens Analytical X-ray Instrument Inc., Madison, WI. 1996; SHELXTL, Version 5.1, Siemens Industrial Automation, Inc., 1997.
[8] H.W. Hou, X. Meng, Y.L. Song, Y.T. Fan, Y. Zhu, H.J. Lu, C.X. Du, W.H. Shao, Inorg. Chem. 41 (2002) 4068.
[9] J.A. Real, M.C. Muñoz, E. Andrés, T. Granier, B. Gallois, Inorg. Chem. 33 (1994) 3587.
[10] (a) G.M. Whitesides, J.P. Mathias, C.T. Seto, Science 254 (1991) 1312;
(b) A.J. Blake, N.R. Champness, A.N. Khlobystov, D.A. Lemenovskii, W.S. Li, M. Schroder, Chem. Commun. (1997) 1339;
(c) H.P. Wu, C. Janiak, L. Uehlin, P. Klufers, P. Mayer, Chem. Commun. 45 (1998) 2637;
(d) Y.P. Cai, H.X. Zhang, A.W. Xu, C.Y. Su, C.L. Chen, J.Q. Liu, L. Zhang, B.S. Kang, J. Chem. Soc. Dalton Trans. 45 (2001) 2429.
[11] A.H. Norbury, Adv. Inorg. Chem. Radiochem. 5 (1975) 17.